# Application of the CBF Method to the Scattering by Combinations of Bodies of Revolution and Arbitrarily Shaped Structures

*Andrzej A. KUCHARSKI*

Telecommunications and Teleinformatics Department, Wrocław University of Technology,
Wybrzeze Wyspianskiego 27, 50-370 Wrocław, Poland

andrzej.kucharski@pwr.wroc.pl

**Abstract.** *In this paper, an algorithm is described which enables efficient analysis of electromagnetic scattering by configurations consisting of arbitrarily shaped conducting bodies and conducting bodies of revolution (BoR). The well-known problem resulting from the loss of azimuthal mode decoupling, when in addition to BoR geometry there exists a body that does not belong to the rotational symmetry of the BoR, is circumvented by the use of characteristic basis function (CBF) method. This however requires careful implementation of the method in order to obtain stable and efficient procedure.*

## Keywords

Method of moments, characteristic basis functions, body of revolution.

## 1. Introduction

One of the well-established method of moments (MoM) variants, enabling efficient analysis of conducting [1], [2], homogeneous dielectric [3], inhomogeneous dielectric [4], [5], or partially inhomogeneous [6] bodies is the method constructed for bodies of revolution, i.e. bodies that can reproduce themselves after rotation by an arbitrary angle with respect to some symmetry axis. The fact that all electromagnetic quantities involved in the analysis (fields, currents, charges) are periodic functions of the "azimuthal" variable, enables representing them in the form of Fourier series, each term of which being so-called "azimuthal mode". Moreover, the Maxwell equations for each azimuthal mode decouple, enabling mode-by-mode analysis, with the number of unknowns in the final linear system of the MoM being only a fraction of the number of unknowns in the system resulting from application of for instance roof-top Rao-Wilton-Glisson (RWG) basis functions [7] in a general purpose code. The obvious drawback is the necessity to solve several such systems, depending on the contribution of the incident fields into the excitation vectors of modal equations. Unfortunately, the presence of a non-BoR part in the configuration spoils this useful feature, introducing the coupling between different modes [8–10]. This results in the description of the problem in terms of one large system of equations, instead of several small ones, thus annihilating to some extent the efficiency of the method. Noting the particular structure of the impedance matrix, one may however avoid the necessity of solving the entire system in one step, making use of the method based upon partitioning [9]. It is also possible to apply an iterative technique [10], based on repeatedly solving the equations for currents on BoR and then on 3D objects, treating fields from currents computed in the previous step as a part of the incident field. Here, we show that another attractive solution is the application of characteristic basis functions method [11], which enables an iteration-free [12] solution of such problems without the necessity of solving large systems of equations, and with preserving useful features associated with the BoR approach. It is to be mentioned the CBF method was previously used in conjunction with the BoR algorithm [13] to solve large BoR problems, here however we apply it to analyze mixed BoR-3D configurations. Here, "3D" stands for "three-dimensional", meaning "non-BOR", part of the geometry, underlining the features of the final equation set that suggest the application of the CBF method.

The rest of this article is organized as follows. First, we will outline the standard BoR-3D formulation [8], [9], [10]. Then we will discuss problems associated with the implementation of the method, giving the special attentions to the features affecting the CBF algorithm. Finally, we will validate the method and check the efficiency of the new algorithm using proper computational examples.

Let's consider situation depicted in Fig. 1, where there are two scatterers, made of perfect electric conductor (PEC), immersed in the incident field $\boldsymbol{E}^i, \boldsymbol{H}^i$. One of the scatterers (BoR) is characterized by rotational symmetry, the second one (3D) has an arbitrary shape. As the starting point of the derivation, we will take the Electric Field Integral Equation (EFIE), which states that the tangential component of the total electric field, being the sum of the incident $\mathbf{E}^i$ and scattered $\mathbf{E}^s$ part, vanishes at the surface of both PEC objects

$$\left(\mathbf{E}^i(\mathbf{r})+\mathbf{E}^s(\mathbf{r})\right)_{tan}=0,\ \ \mathbf{r}\in S. \tag{1}$$

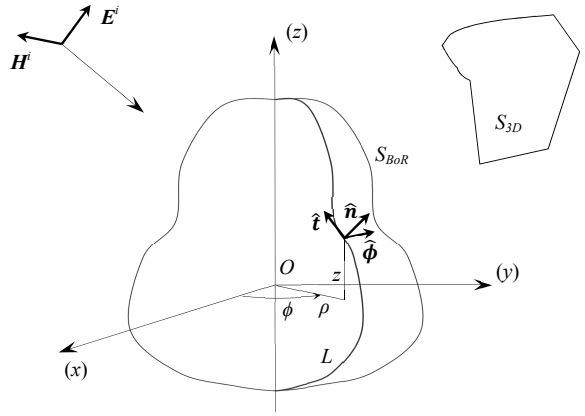


**Fig. 1.** Scattering by a combined BoR/3D geometry.

## 2. Standard Algorithm

The scattered field may be calculated using mixed-potential representation (cf. [7])

$$\mathbf{E}^s(\mathbf{r})=-j\omega\mathbf{A}(\mathbf{r})-\nabla\Phi(\mathbf{r}) \tag{2}$$

where

$$\mathbf{A}(\mathbf{r})=\frac{\mu_0}{4\pi}\int_S \mathbf{J}(\mathbf{r}')\frac{e^{-jk|\mathbf{r}-\mathbf{r}'|}}{|\mathbf{r}-\mathbf{r}'|}dS', \tag{3}$$

$$\Phi(\mathbf{r})=\frac{1}{4\pi\varepsilon_0}\int_S q(\mathbf{r}')\frac{e^{-jk|\mathbf{r}-\mathbf{r}'|}}{|\mathbf{r}-\mathbf{r}'|}dS', \tag{4}$$

$$q(\mathbf{r}')=-\frac{\nabla\cdot\mathbf{J}(\mathbf{r}')}{j\omega}. \tag{5}$$

Above, $k$ is the wavenumber, $\mathbf{r}$ and $\mathbf{r}'$ indicate observation and source points, respectively, while the integration domain $S=S_{BoR}\cup S_{3D}$ is the geometrical sum of surfaces defining both BoR and 3D objects. Equation (1) is transformed into a linear equation set by first approximating the unknown current density with the properly chosen basis functions, and then by applying the testing procedure. Here, we apply the usual RWG basis functions to represent current density on the non-BoR object

$$\mathbf{J}^{3D}(\mathbf{r}')=\sum_{n=1}^{N_{3D}} I_n^{3D}\Lambda_n^{RWG}(\mathbf{r}'),\ \ \mathbf{r}'\in S_{3D}, \tag{6}$$

while for the current on the BoR, we use the expansion (cf. [14])

$$\mathbf{J}^{BoR}(\mathbf{r}')=\sum_{p=-P}^{P}\left(\sum_{n=1}^{N_t} I_n^{t,p}\frac{1}{\rho'}\Lambda_n(t')\hat{\mathbf{t}}'+\sum_{n=1}^{N_\phi} I_n^{\phi,p}\Pi_n(t')\hat{\boldsymbol{\phi}}'\right)e^{jp\phi'},\ \ \mathbf{r}'\in S_{BoR}. \tag{7}$$

In (7), $\mathbf{r}'$ is expressed in cylindrical coordinates as $\mathbf{r}'=(\rho',z',\phi')=(t',\phi')$, where $t'$ denotes the source point at the *generating arc* of the BoR. $\Lambda_n(t')$ and $\Pi_n(t')$ are respectively triangle and pulse functions along the generating arc, unit vectors $\hat{\mathbf{t}}'$ and $\hat{\boldsymbol{\phi}}'$ define the tangential (to $S_{BoR}$) current components at $\mathbf{r}'$, and $p=-P,...,0,...,P$ denotes the *azimuthal mode* defining current variation along the $\phi'$ coordinate. Maximum number of azimuthal modes is described by $P$, which depends on the wavenumber, maximum radius of the BoR, and the modal composition of the incident field. In the MoM procedure, we use testing functions, which for the non-BoR surface are again RWG roof-tops, while for the field at the surface of the BoR, we apply functions being the complex conjugates of functions present in (7).

Finally, we arrive at the matrix equation (cf. [8] – [10])

$$\left[\begin{array}{cccc|c} \mathbf{Z}_{B,B}^{-P} & 0 & \cdots & 0 & \mathbf{Z}_{B,3D}^{-P} \\ 0 & \mathbf{Z}_{B,B}^{p} & 0 & \vdots & \mathbf{Z}_{B,3D}^{p} \\ \vdots & 0 & \ddots & 0 & \vdots \\ 0 & \cdots & 0 & \mathbf{Z}_{B,B}^{P} & \mathbf{Z}_{B,3D}^{P} \\ \hline \mathbf{Z}_{3D,B}^{-P} & \mathbf{Z}_{3D,B}^{p} & \cdots & \mathbf{Z}_{3D,B}^{P} & \mathbf{Z}_{3D,3D} \end{array}\right]\left[\begin{array}{c} \mathbf{I}_B^{-P} \\ \mathbf{I}_B^{p} \\ \vdots \\ \mathbf{I}_B^{P} \\ \hline \mathbf{I}_{3D} \end{array}\right] = \left[\begin{array}{c} \mathbf{V}_B^{-P} \\ \mathbf{V}_B^{p} \\ \vdots \\ \mathbf{V}_B^{P} \\ \hline \mathbf{V}_{3D} \end{array}\right] \tag{8}$$

where sub-matrices with $B,B$ and $3D,3D$ indices describe self interactions of BoR and 3D objects, respectively, mixed subscripts denote interactions between BoR and 3D, and superscripts refer to azimuthal modes at BoR. Zeros in the BoR-BoR part of the impedance matrix come from the well-known decoupling of azimuthal modes (cf. [1], [2]).

Also

$$\mathbf{Z}_{B,B}^{p}=\left[\begin{array}{cc} \mathbf{Z}_{t,t}^{p} & \mathbf{Z}_{t,\phi}^{p} \\ \mathbf{Z}_{\phi,t}^{p} & \mathbf{Z}_{\phi,\phi}^{p} \end{array}\right]=\left[\begin{array}{cc} \left[Z_{mn}^{t,t,p}\right] & \left[Z_{mn}^{t,\phi,p}\right] \\ \left[Z_{mn}^{\phi,t,p}\right] & \left[Z_{mn}^{\phi,\phi,p}\right] \end{array}\right], \tag{9}$$

$$\mathbf{Z}_{B,3D}^{p}=\left[\begin{array}{c} \mathbf{Z}_{t,3D}^{p} \\ \mathbf{Z}_{\phi,3D}^{p} \end{array}\right]=\left[\begin{array}{c} \left[Z_{mn}^{t,3D,p}\right] \\ \left[Z_{mn}^{\phi,3D,p}\right] \end{array}\right], \tag{10}$$

$$\mathbf{Z}_{3D,B}^{p}=\left[\begin{array}{cc} \mathbf{Z}_{3D,t}^{p} & \mathbf{Z}_{3D,\phi}^{p} \end{array}\right]=\left[\begin{array}{cc} \left[Z_{mn}^{3D,t,p}\right] & \left[Z_{mn}^{3D,\phi,p}\right] \end{array}\right], \tag{11}$$

$$\mathbf{Z}_{3D,3D}=\left[Z_{mn}^{3D,3D}\right]. \tag{12}$$

Vectors grouping unknowns are defined as

$$\mathbf{I}_B^{p}=\left[\begin{array}{c} \mathbf{I}_t^{p} \\ \mathbf{I}_\phi^{p} \end{array}\right]=\left[\begin{array}{c} \left[I_n^{t,p}\right] \\ \left[I_n^{\phi,p}\right] \end{array}\right], \tag{13}$$

$$\mathbf{I}_{3D} = \left[I_n^{3D}\right], \tag{14}$$

while for the excitation vectors we use the notation

$$\mathbf{V}_B^p = \begin{bmatrix} \mathbf{V}_t^p \\ \mathbf{V}_\phi^p \end{bmatrix} = \begin{bmatrix} \left[V_m^{t,p}\right] \\ \left[V_m^{\phi,p}\right] \end{bmatrix}, \tag{15}$$

$$\mathbf{V}_{3D} = \left[V_m^{3D}\right]. \tag{16}$$

In above formulas indices $m$ and $n$ take values between 1 and the appropriate number of basis/testing functions, i.e. $N_t$ or $N_\phi$ for BoR related approximations and $N_{3D}$ for non-BoR ones.

Matrix elements in (9) and (10) are obtained from

$$\begin{aligned} Z_{mn}^{t,u,p} &= -\int_{S_{BoR}} \mathbf{E}_n^{s,u} \cdot \hat{\mathbf{t}} \frac{\Lambda_m}{\rho} e^{-jp\phi} dS \\ &= \int_{S_{BoR}} \left( j\omega \mathbf{A}_n^u \cdot \hat{\mathbf{t}} \frac{\Lambda_m}{\rho} - \Phi_n^u \frac{\partial \Lambda_m}{\partial t} \right) e^{-jp\phi} dS, \end{aligned} \tag{17}$$

$$\begin{aligned} Z_{mn}^{\phi,u,p} &= -\int_{S_{BoR}} \mathbf{E}_n^{s,u} \cdot \hat{\boldsymbol{\phi}} \Pi_m e^{-jp\phi} dS \\ &= \int_{S_{BoR}} \left( j\omega \mathbf{A}_n^u \cdot \hat{\boldsymbol{\phi}} \Pi_m + \frac{jp}{\rho} \Phi_n^u \Pi_m \right) e^{-jp\phi} dS \end{aligned} \tag{18}$$

where $u = t, \phi$ or $3D$, $\mathbf{E}_n^{s,u}$ is the electric field produced by the current corresponding to a single basis function, and potentials $\mathbf{A}_n^u$ and $\Phi_n^u$ are calculated from (3)–(5) substituting for $\mathbf{J}$, respectively, $\frac{1}{\rho'} \Lambda_n \hat{\mathbf{t}}' e^{jp\phi'}$, $\Pi_n \hat{\boldsymbol{\phi}}' e^{jp\phi'}$, $\Lambda_n^{RWG}$, and for $S$ either $S_{BoR}$ or $S_{3D}$. Obviously, the surface integrals in formulas describing the BoR–BoR interactions finally reduce to line integrals along generating arc $L$, while integrals with respect to the azimuthal variable define *modal Green's functions* [1], [2].

Elements of (11) are calculated from

$$\begin{aligned} Z_{mn}^{3D,u,p} &= -\int_{S_{3D}} \mathbf{E}_n^{s,u} \cdot \Lambda_m^{RWG} dS \\ &= \int_{S_{3D}} \left( j\omega \mathbf{A}_n^u \cdot \Lambda_m^{RWG} - \Phi_n^u \nabla \cdot \Lambda_m^{RWG} \right) dS, \end{aligned} \tag{19}$$

with $u = t, \phi$, and finally elements of (12) are given as

$$\begin{aligned} Z_{mn}^{3D,3D} &= -\int_{S_{3D}} \mathbf{E}_n^{s,3D} \cdot \Lambda_m^{RWG} dS \\ &= \int_{S_{3D}} \left( j\omega \mathbf{A}_n^{3D} \cdot \Lambda_m^{RWG} - \Phi_n^{3D} \nabla \cdot \Lambda_m^{RWG} \right) dS. \end{aligned} \tag{20}$$

Excitation vector entries are given by

$$V_m^{t,p} = \int_{S_{BoR}} \mathbf{E}^i \cdot \hat{\mathbf{t}} \frac{\Lambda_m}{\rho} e^{-jp\phi} dS, \tag{21}$$

$$V_m^{\phi,p} = \int_{S_{BoR}} \mathbf{E}^i \cdot \hat{\boldsymbol{\phi}} \Pi_m e^{-jp\phi} dS, \tag{22}$$

$$V_m^{3D} = \int_{S_{3D}} \mathbf{E}^i \cdot \Lambda_m^{RWG} dS. \tag{23}$$

One can note that several Fourier integrals are contained in the above formulas, which may be calculated efficiently using FFT [13], [15].

As seen from (8), the presence of the 3D body introduces the coupling between azimuthal modes of the BoR, thus enforcing the necessity of solving one large matrix equation, instead of several small sets in a typical mode-by-mode BoR solution scheme. As mentioned in the introduction, one solution to this problem is the application of partitioning at the stage of solving the final matrix equation [9], which leads to the necessity of inversion of matrices with the size of diagonal blocks present in (8). In [10], it is proposed to use the iterative technique based upon taking as a first approximation for non-BoR current the solution resulting from physical optics approach, then using field produced by that current, together with the original excitation field, to obtain the current on BoR, then reversing the procedure, i.e. using field produced by BoR current, together with the original excitation field, to obtain the new approximation to non-BoR current, and so on. In [10] it is also mentioned the possibility of using iterative method, like Gauss-Seidel or conjugate gradient, to solve (8). This approach may benefit from large blocks of zeros in the impedance matrix, which makes faster the computation of matrix-vector products present in the algorithms.

# 3. Application of the CBF Method

Let's re-write the matrix equation (8) in the simplified form, i.e. without sub-division into particular BoR azimuthal modes

$$\left[\begin{array}{c|c} \mathbf{Z}_{B,B} & \mathbf{Z}_{B,3D} \\ \hline \mathbf{Z}_{3D,B} & \mathbf{Z}_{3D,3D} \end{array}\right] \left[\begin{array}{c} \mathbf{I}_B \\ \hline \mathbf{I}_{3D} \end{array}\right] = \left[\begin{array}{c} \mathbf{V}_B \\ \hline \mathbf{V}_{3D} \end{array}\right]. \tag{24}$$

In the CBF method [11], [12], we first calculate so-called *primary* basis functions being the approximations of currents on both objects, computed neglecting mutual interactions, from equations

$$\mathbf{Z}_{B,B} \cdot \mathbf{I}_B^{(1)} = \mathbf{V}_B, \tag{25}$$

$$\mathbf{Z}_{3D,3D} \cdot \mathbf{I}_{3D}^{(1)} = \mathbf{V}_{3D}. \tag{26}$$

It is to be noted that the primary basis functions, defined by the coefficients obtained from above equations, are valid for the excitation from the original problem, as in [11]. The possibility introduced in [12], where – for scattering problems – primary basis functions are computed using as excitations waves incoming from different angles, is

not considered here. The problem of forming excitation-independent characteristic basis functions for BoR/3D configurations can be the subject of further study.

Next, we introduce the *secondary* basis functions, as the currents induced on each object by the field produced by the primary basis function current flowing on the other object, which are described by equations

$$\mathbf{Z}_{B,B}\cdot\mathbf{I}_B^{(2)} = -\mathbf{Z}_{B,3D}\cdot\mathbf{I}_{3D}^{(1)}, \tag{27}$$

$$\mathbf{Z}_{3D,3D}\cdot\mathbf{I}_{3D}^{(2)} = -\mathbf{Z}_{3D,B}\cdot\mathbf{I}_B^{(1)}. \tag{28}$$

If there is a need, one may also introduce the *tertiary* basis functions, satisfying

$$\mathbf{Z}_{B,B}\cdot\mathbf{I}_B^{(3)} = -\mathbf{Z}_{B,3D}\cdot\mathbf{I}_{3D}^{(2)}, \tag{29}$$

$$\mathbf{Z}_{3D,3D}\cdot\mathbf{I}_{3D}^{(3)} = -\mathbf{Z}_{3D,B}\cdot\mathbf{I}_B^{(2)}. \tag{30}$$

The computed primary, secondary, and optionally tertiary basis functions may be then used as new basis and testing functions to form the set with only four (without tertiaries) or six (with tertiaries) unknowns. We also note that computing $\mathbf{I}_B^{(l)}, l = 1,2,3$ vectors with matrix equations (25), (27), (29), in view of block diagonal character of $\mathbf{Z}_{B,B}$, remains within BoR scheme, so it can be done in the mode-by-mode manner. One may wonder, why not use as new macro basis functions the currents on BoR associated with particular modes. It is possible, but it doesn't speed-up computations, as the only difference is splitting $\mathbf{I}_B^{(l)}$ vectors into several smaller parts, which only results in the larger final equation set. The non-trivial part is in the considered case forming the final matrix equation in order to obtain coefficients standing in front of characteristic basis functions in the resulting approximation. To accomplish this, one has to bear in mind that the characteristic basis functions are the distributions of the current densities, described with the coefficients forming vectors $\mathbf{I}_B^{(l)}$ or $\mathbf{I}_{3D}^{(l)}$, and not the vectors themselves. In other words, the CBF method is the method developed to solve electromagnetic problem, and not to solve the resulting linear equation set. Thus, we have the following general equations for the new impedance matrix and excitation vector elements

$$Z_{CBF}{}_{ji}^{B,B} = -\int_{S_{BoR}} \mathbf{E}^s\left(\mathbf{J}_B^{(i)}\right)\cdot\mathbf{J}_B^{(j)}dS, \tag{31}$$

$$Z_{CBF}{}_{ji}^{B,3D} = -\int_{S_{BoR}} \mathbf{E}^s\left(\mathbf{J}_{3D}^{(i)}\right)\cdot\mathbf{J}_B^{(j)}dS, \tag{32}$$

$$Z_{CBF}{}_{ji}^{3D,B} = -\int_{S_{3D}} \mathbf{E}^s\left(\mathbf{J}_B^{(i)}\right)\cdot\mathbf{J}_{3D}^{(j)}dS, \tag{33}$$

$$Z_{CBF}{}_{ji}^{3D,3D} = -\int_{S_{3D}} \mathbf{E}^s\left(\mathbf{J}_{3D}^{(i)}\right)\cdot\mathbf{J}_{3D}^{(j)}dS, \tag{34}$$

$$V_{CBF}{}_{j}^{B} = \int_{S_{BoR}} \mathbf{E}^i\cdot\mathbf{J}_B^{(j)}dS, \tag{35}$$

$$V_{CBF}{}_{j}^{3D} = \int_{S_{3D}} \mathbf{E}^i\cdot\mathbf{J}_{3D}^{(j)}dS \tag{36}$$

where $\mathbf{J}_{3D}^{(l)}$ and $\mathbf{J}_B^{(l)}$, $l = i, j$, are the current density distributions described, respectively, by (6) and (7) with approximation coefficients $\mathbf{I}_{3D}^{(l)}$ and $\mathbf{I}_B^{(l)}$. Computation of (33) and (34), as well as (36) is straightforward:

$$Z_{CBF}{}_{ji}^{3D,B} = \left(\mathbf{I}_{3D}^{(j)}\right)^T\mathbf{Z}_{3D,B}\cdot\mathbf{I}_B^{(i)}, \tag{37}$$

$$Z_{CBF}{}_{ji}^{3D,3D} = \left(\mathbf{I}_{3D}^{(j)}\right)^T\mathbf{Z}_{3D,3D}\cdot\mathbf{I}_{3D}^{(i)}, \tag{38}$$

$$V_{CBF}{}_{j}^{3D} = \left(\mathbf{I}_{3D}^{(j)}\right)^T\mathbf{V}_{3D}. \tag{39}$$

This is however not the case when considering (31), (32), and (35). The problem lies in the fact that when computing entries of $\mathbf{Z}_{B,B}$, we use $e^{jp\phi'}$ modal dependence in basis functions, while $e^{-jp\phi}$ in testing functions. On the other hand, when using CBFs defined on BoR, we have in both cases $e^{jp\phi'}$ and $e^{jp\phi}$, respectively. Similarly, elements of $\mathbf{Z}_{B,3D}$ and of $\mathbf{V}_B$ in (24) are calculated using $e^{-jp\phi}$-dependent testing functions, and in (32) and (35) we use functions with $e^{jp\phi}$ term.

To illustrate this, let's consider the formula (31). After substituting for the basis and testing functions their modal expansions, we get

$$Z_{CBF}{}_{ji}^{B,B} = -\int_{S_{BoR}} \mathbf{E}^s\left(\sum_{r=-P}^{P}\mathbf{J}_B^{r,(i)}e^{jr\phi'}\right)\cdot\left(\sum_{p=-P}^{P}\mathbf{J}_B^{p,(j)}e^{jp\phi}\right)dS \tag{40}$$

where, according to (7),

$$\mathbf{J}_B^{r,(i)} = \sum_{n=1}^{N_t} I_n^{t,r,(i)}\frac{1}{\rho'}\Lambda_n\left(t'\right)\hat{\mathbf{t}}' + \sum_{n=1}^{N_\phi} I_n^{\phi,r,(i)}\Pi_n\left(t'\right)\hat{\phi}' \tag{41}$$

is the part of the $i$-th CBF defined on BoR, corresponding to the azimuthal mode $r$, and without the exponential term. $\mathbf{J}_B^{p,(j)}$ is given by the similar formula, with source coordinates replaced by observation point (non-primed) ones, $r$ replaced by $p$, and $(i)$ replaced by $(j)$.

Invoking the orthogonality of azimuthal harmonics, we find that only modes with $r = -p$ contribute to the integral (40), which yields

$$Z_{CBF}{}_{ji}^{B,B} = -\int_{S_{BoR}}\sum_{p=-P}^{P}\mathbf{E}^{s,-p,(i)}\cdot\mathbf{J}_B^{p,(j)}dS \tag{42}$$

where $\mathbf{E}^{s,-p,(i)}$ is the field produced by $\mathbf{J}_B^{-p,(i)}e^{-jp\phi'}$.

After exchanging the integral and summation symbols, we may express (42) in terms of, already computed, matrices

$$Z_{CBF}{}_{ji}^{B,B} = \sum_{p=-P}^{P} \left(\mathbf{I}_B^{p,(j)}\right)^T \mathbf{Z}_{B,B}^{-p} \cdot \mathbf{I}_B^{-p,(i)} \tag{43}$$

where $\mathbf{I}_B^{p,(j)}$ and $\mathbf{I}_B^{-p,(i)}$ are proper "modal" parts of vectors $\mathbf{I}_B^{(j)}$ and $\mathbf{I}_B^{(i)}$, respectively.

We can also put (43) into matrix form similar to (37), (38):

$$Z_{CBF}{}_{ji}^{B,B} = \left(\mathbf{I}_B^{(j)}\right)^T \mathbf{Y}_{B,B} \cdot \mathbf{I}_B^{(i)} \tag{44}$$

where

$$\mathbf{Y}_{B,B} = \begin{bmatrix} 0 & \cdots & 0 & \mathbf{Z}_{B,B}^{P} \\ \vdots & 0 & \iddots & 0 \\ 0 & \mathbf{Z}_{B,B}^{p} & 0 & \vdots \\ \mathbf{Z}_{B,B}^{-P} & 0 & \cdots & 0 \end{bmatrix}. \tag{45}$$

Similar consideration can be performed to obtain matrix formulas needed to calculate $Z_{CBF}{}_{ji}^{B,3D}$ and $V_{CBF}{}_{j}^{B}$:

$$Z_{CBF}{}_{ji}^{B,3D} = \left(\mathbf{I}_B^{(j)}\right)^T \mathbf{Y}_{B,3D} \cdot \mathbf{I}_{3D}^{(i)}, \tag{46}$$

$$V_{CBF}{}_{j}^{B} = \left(\mathbf{I}_B^{(j)}\right)^T \mathbf{U}_{3D} \tag{47}$$

where

$$\mathbf{Y}_{B,3D} = \begin{bmatrix} \mathbf{Z}_{B,3D}^{P} \\ \vdots \\ \mathbf{Z}_{B,3D}^{p} \\ \mathbf{Z}_{B,3D}^{-P} \end{bmatrix}, \tag{48}$$

$$\mathbf{U}_B = \begin{bmatrix} \mathbf{V}_B^{P} \\ \vdots \\ \mathbf{V}_B^{p} \\ \mathbf{V}_B^{-P} \end{bmatrix}. \tag{49}$$

Note that in $\mathbf{Y}_{B,B}$, $\mathbf{Y}_{B,3D}$ and $\mathbf{U}_B$ the order of block rows is inverted in comparison to $\mathbf{Z}_{B,B}$, $\mathbf{Z}_{B,3D}$ and $\mathbf{V}_B$. It is also to be noted that despite the notation used in (44), in the code implementing the method we have made use of block structure of $\mathbf{Y}_{B,B}$, multiplying only non-zero blocks and corresponding parts of proper CBFs, which corresponds to direct application of (43).

Above, it has been indicated that the main problem in the direct application of the CBF method to BoR/3D structures is in the opposite sign in the exponential term in the definition of original BoR testing functions, and in corresponding CBFs, when symmetric product is used in the construction of CBF MoM matrix. This problem obviously would not appear if we had used scalar product instead. In that case complex conjugate of testing functions would be applied, resulting in automatic inversion of the sign of exponential terms in BoR CBFs. Such procedure was also implemented, however led to less accurate results. One explanation of this may be included in Wang's statement ( [16], p. 15) that the application of symmetric product is often considered superior to the scalar product, as the resulting matrix equation is also a statement of reciprocity. This problem however requires further investigation.

# 4. Computational Examples

In order to validate the procedure described in Section 3, the test configuration depicted in Fig. 2 has been used. The geometry consists of the square plate, which is considered 3D body, and the sphere constituting BoR. Three computational models have been used, with symmetry axis along $x$, $y$, and $z$-axis, which correspond to different modal expansions of fields and currents associated with the BoR, describing at the same time exactly the same physical situation. For symmetry axis along $z$, we need only two $p = \pm 1$ azimuthal modes to be taken into account. For other cases the number of modes depends on the wavenumber and maximum radial size of the BoR. Here, we consider maximum $ka = 10.0$, so according to [14], we have to include modes with $p = -10, ..., 10$ .

In the computations, the plate was divided into 2312 triangles, which generated 3400 RWG basis functions, the BoR generating arc was divided into 60 segments, which gave 119 unknowns per azimuthal mode. Integrations along the azimuthal variable were done using 128 samples. In the first computational cycle, we put the BoR symmetry axis along $z$-axis. Thus, the total number of unknowns was $3400 + 2 \cdot 119 = 3638$. In this particular case, the CBF method is not expected to be much more efficient than the direct solution, however it is useful as the tool for the validation of the procedure. Next, we have applied the algorithm to the case, when BoR (sphere) symmetry axis is along $x$ or $y$-axis. In both cases, we have $3400 + 21 \cdot 119 = 5899$ unknowns in the resulting linear set. The results of the computations are shown in Fig. 3, where there are also included comparison data obtained with FEKO [17]. In the figure, symbol in parenthesis denotes BoR symmetry axis used in the computations. One can see that the agreement of the results is very good. At this validation stage it was also found that for higher frequencies tertiary CBFs mentioned in the previous section had to be used.

It is to be noted that in the example, the electric field integral equation (EFIE) has been used to model both open and closed bodies, while it is well known [18] that for closed bodies EFIE formulation suffers from the spurious resonance problem. However, it was not experienced here, which may be attributed to the fact that spurious part of the resonant current produces no field outside the closed object [18]. As a result, possible inaccuracies do not manifest themselves in radar cross section plots. Nevertheless, the described procedure can be generalized to include the combined field integral equation (CFIE) for closed parts of the combined geometry [19], as it would only affect the formulas used to

compute entries of the (original) MoM matrix and of the excitation vector.

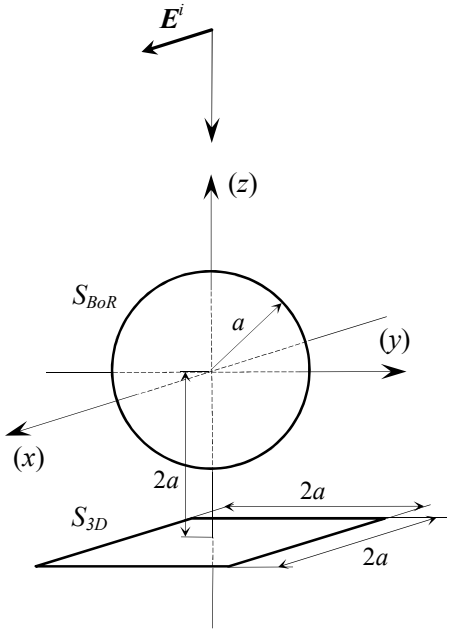


**Fig. 2.** Scattering from a sphere accompanied by a square plate.

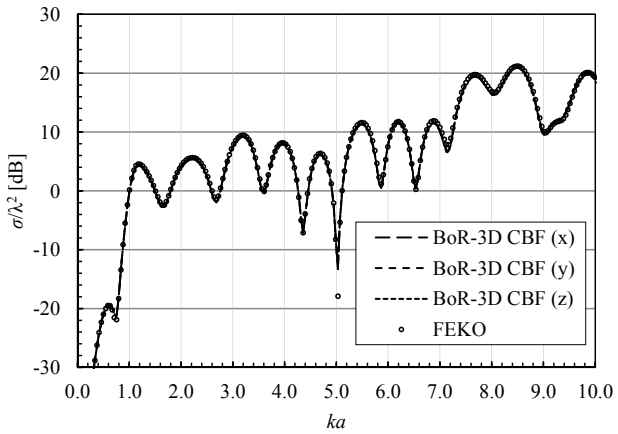


**Fig. 3.** Radar cross section of the sphere/square plate configuration.

Next, the algorithm has been applied to the problem from the class for which the method is especially well suited – the geometry composed of electrically large BoR and small (in the terms of number of unknowns) 3D body. Such an example is depicted in Fig. 4, where we have large conducting sphere and narrow metal strip with the length the same as the sphere diameter. In order to avoid $p = \pm 1$ configuration, the symmetry axis of the BoR has been chosen along $z$ axis. The problem has been analyzed up to $ka = 20.0$, so modes with $p = -20, ..., 20$ have been taken into account. The generating arc of the sphere was divided into 90 segments, which resulted in $159 + 41 \cdot 179 = 7498$ unknowns, where 159 was the number of RWG functions used to model the strip. The comparison of results is given in Fig. 5.

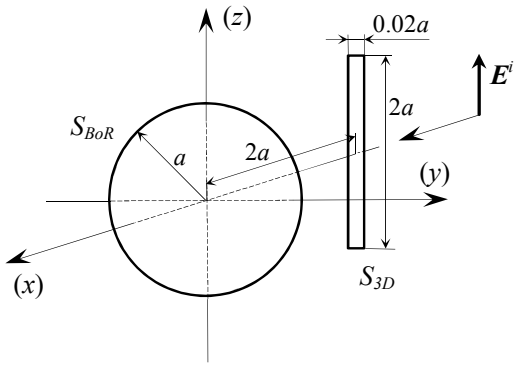


**Fig. 4.** A sphere accompanied by a narrow strip.

The computations were performed on the 2 processors/8 cores Intel®Xeon®X5472 3.00 GHz workstation using numbers of cores equal to 1, 4 and 8. It is to be noted that the parallelization in the author's code came from Intel®MKL library used. The reference model was again done in FEKO using single precision storage and program-suggested meshing – this resulted in the total number of 43757 unknowns. FEKO calculations were performed using 1 and 4 cores, allowed by the single processor license. The computation times are listed in Tab. 1, where "BoR-3D LU" stands for the code with standard LU decomposition method used to solve the linear set (8), while "BoR-3D CBF" is the application of the method from Section 3.

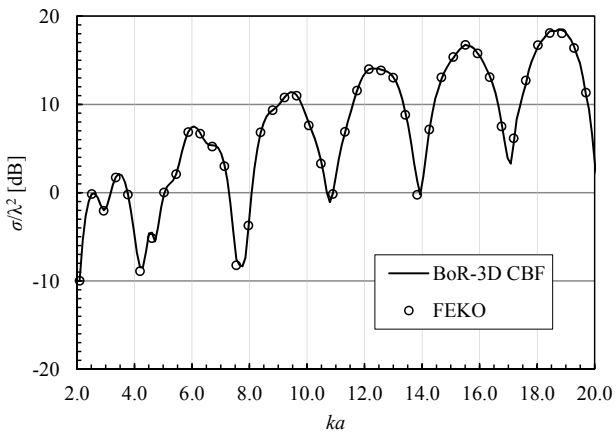


**Fig. 5.** Radar cross section of the sphere/strip configuration.

It is to be noted that even without applying CBFs, the BOR-3D algorithm was very efficient, which resulted from much less number of unknowns required to describe the problem than in the standard 3D method with RWG basis functions.

When CBFs were used we noted that the time needed at the linear system solution stage was reduced from 130 (1 core) to more than 17 (8 cores) times, noting once again that in the author's code the only parallelization came from Intel®MKL library. Slightly shorter matrix filling time in the case of the CBF method came from the fact that in that case it was no need to copy modal moment matrix blocks to one big matrix. The comparison of results is given in Fig. 5, where FEKO results, computed using larger frequency intervals, are depicted with circles. Again the agreement is

excellent, while the total computation time (4 cores) was 64.9 hours (for 46 frequencies) for the case of FEKO and 64 minutes (for 181 frequencies) for the present method. This once again proves that the BoR-3D CBF algorithm may be useful for that type of configurations.

| Code | Cores | Matrix fill | Solution | Total |
|---|---|---|---|---|
| BOR-3D LU | 1 | 22s | 104s | 126s |
| BOR-3D CBF | 1 | 19.2s | 0.8s | 20s |
| FEKO | 1 | 58.7min | 171.9min | 230.6min |
| BOR-3D LU | 4 | 21.3s | 27.3s | 48.6s |
| BOR-3D CBF | 4 | 18.8s | 0.8s | 19.6s |
| FEKO | 4 | 21.2min | 62.4min | 83.7min |
| BOR-3D LU | 8 | 21.4s | 14s | 35.4s |
| BOR-3D CBF | 8 | 18.6s | 0.8s | 19.4s |

**Tab. 1.** Computation times (single frequency) for the problem from Fig. 4.

# 5. Conclusions

In this paper the Characteristic Basis Functions method was used to efficiently model scattering from two perfectly conducting bodies, one of them constituting a body-of-revolution. It was shown that the proposed method is very efficient in cases, when large BoR is accompanied by a relatively small general shape 3D object.

Further developments could concern generalization of the method into multiple body analysis, radiation problems [20], or analysis of dielectric bodies. Another problem that should be addressed is including junctions between BoR and 3D parts [8], [10].

# References


[1] ANDREASEN, M. G. Scattering from bodies of revolution. *IEEE Transactions on Antennas and Propagation*, 1965, vol. 13, no. 2, p. 303 - 310.

[2] MAUTZ, J. R., HARRINGTON, R. F. Radiation and scattering from bodies of revolution. *Applied Scientific Research*, 1969, vol. 20, no. 1, p. 405 - 435.

[3] MAUTZ, J. R., HARRINGTON, R. F. Electromagnetic scattering from a homogeneous material body of revolution. *Archiv fuer Elektronik und Uebertragungstechnik*, 1979, vol. 33, p. 71 - 80.

[4] GOVIND, S., WILTON, D. R., GLISSON A. W. Scattering from inhomogeneous penetrable bodies of revolution. *IEEE Transactions on Antennas and Propagation*, 1984, vol. 32, no. 11, p. 1163 - 1173.

[5] KUCHARSKI, A. A. A method of moments solution for electromagnetic scattering by inhomogeneous dielectric bodies of revolution. *IEEE Transactions on Antennas and Propagation*, 2000, vol. 48, no. 8, p. 1202 - 1210.

[6] KUCHARSKI, A. A. Electromagnetic scattering by partially inhomogeneous dielectric bodies of revolution. *Microwave and Optical Technology Letters*, 2005, vol. 44, no. 3, p. 275 - 281.

[7] RAO, S. M., WILTON, D. R., GLISSON, A. W. Electromagnetic scattering by surfaces of arbitrary shape. *IEEE Transactions on Antennas and Propagation*, 1982, vol. 30, no. 3, p. 409 - 418.

[8] SHAEFFER, J. F., MEDGYESI-MITSCHANG, L. N. Radiation from wire antennas attached to bodies of revolution: the junction problem. *IEEE Transactions on Antennas and Propagation*, 1981, vol. 29, no. 3, p. 479 - 487.

[9] DURHAM, T. E., CHRISTODOULOU, C. G. Electromagnetic radiation from structures consisting of combined body of revolution and arbitrary surfaces. *IEEE Transactions on Antennas and Propagation*, 1992, vol. 40, no. 9, p. 1061 - 1067.

[10] SULLIVAN, A., CARIN, L. Scattering from complex bodies using a combined direct and iterative technique. *IEEE Transactions on Antennas and Propagation*, 1999, vol. 47, no. 1, p. 33 - 39.

[11] PRAKASH, V. V. S., MITTRA, R. Characteristic basis function method: a new technique for efficient solution of method of moments matrix equation. *Microwave and Optical Technology Letters*, 2003, vol. 36, no. 2, p. 95 - 100.

[12] MITTRA, R., DU, K. Characteristic basis function method for iteration-free solution of large method of moments problems. *Progress In Electromagnetics Research B*, 2008, vol. 6, p. 307 - 336.

[13] MITTRA, R., LI, S., MA, J.-F. Solving large Body of Revolution (BOR) problems using the Characteristic Basis Function Method and the FFT-based matrix generation. In *IEEE Antennas and Propagation Society International Symposium*. Albuquerque (NM, USA), 2006, p. 3879 - 3882.

[14] WILTON, D. R. Computational Methods. PIKE, R., SABATIER, P. (Eds.) *Scattering*, ch. 1.5.5, Academic Press, 2002.

[15] GEDNEY, S. D., MITTRA, R. The use of the FFT for the efficient solution of the problem of electromagnetic scattering by a body of revolution. *IEEE Transactions on Antennas and Propagation*, 1990, vol. 38, no. 3, p. 313 - 322.

[16] WANG, J. J. H. *Generalized Moment Methods in Electromagnetics*. John Wiley & Sons, 1991.

[17] FEKO Suite 5.4, EM Software and Systems (www.feko.info), 2008.

[18] MAUTZ, J. R., HARRINGTON, R. F. H-field, E-field and combined-field solutions for conducting bodies of revolution. *Archiv fuer Elektronik und Uebertragungstechnik*, 1978, vol. 32, p. 159 - 164.

[19] ERGÜL, Ö., GÜREL, L. Iterative Solution of Composite Problems with the Combined-Field Integral Equation. In *Proceedings of the 36th European Microwave Conference*, 2006, p. 239 - 240.

[20] KUCHARSKI, A. A. Wideband characteristic basis functions in radiation problems. *Radioengineering*, 2012, vol. 21, no. 2, p. 590 - 596.


# About Author ...

**Andrzej A. KUCHARSKI** was born in 1964. He received his M.Sc., Ph.D. and D.Sc. from Wroclaw University of Technology in 1988, 1994, and 2001, respectively. He is the Head of the Antenna Theory and Computational Electromagnetics Group in the Telecommunications and Teleinformatics Department, Faculty of Electronics, Wroclaw University of Technology, Poland. His research interests include computational electromagnetics in radiation and scattering problems.